

HGO-YOLO: Advancing Anomaly Behavior Detection with Hierarchical Features and Lightweight Optimized Detection

Qizhi Zheng, Zhongze Luo, Meiyan Guo, Xinzhu Wang, Renqimuge Wu, Qiu Meng, Guanghui Dong*

College of computer and control engineering, Northeast Forestry University, Harbin, 150040, China

Abstract –

Accurate and real-time object detection is crucial for anomaly behavior detection, especially in scenarios constrained by hardware limitations, where balancing accuracy and speed is essential for enhancing detection performance. This study proposes a model called HGO-YOLO, which integrates the HGNetv2 architecture into YOLOv8. This combination expands the receptive field and captures a wider range of features while simplifying model complexity through GhostConv. We introduced a lightweight detection head, OptiConvDetect, which utilizes parameter sharing to construct the detection head effectively. Evaluation results show that the proposed algorithm achieves a mAP@0.5 of 87.4% and a recall rate of 81.1%, with a model size of only 4.6 MB and a frame rate of 56 FPS on the CPU. HGO-YOLO not only improves accuracy by 3.0% but also reduces computational load by 51.69% (from 8.9 GFLOPs to 4.3 GFLOPs), while increasing the frame rate by a factor of 1.7. Additionally, real-time tests were conducted on Raspberry Pi4 and NVIDIA platforms. These results indicate that the HGO-YOLO model demonstrates superior performance in anomaly behavior detection.

Keywords - YOLOv8, HGNetv2, Lightweight, Anomaly Behavior Detection

1. Introduction

In contemporary society, the detection of anomalous behavior in both public and private buildings has become pervasive, especially with the widespread deployment of cameras and video surveillance systems. These systems are engineered to monitor for abnormal behavior to identify potential threats or safety hazards, which is a crucial aspect of maintaining public safety. However, traditional surveillance systems depend a lot on human operators. They need these operators to watch video feeds. This can lead to inefficiencies because of human traits. These traits include fatigue and lapses in concentration. These factors often lead to missed events or slow responses. This can make it hard to detect potential threats on time. It also reduces the effectiveness of keeping public safety and peace.

Intelligent detection systems have been developed to meet this challenge. These systems can automatically find different types of abnormal behavior. This paper will explore three common situations for detecting abnormal behavior. These situations are falling, fighting, and smoking[1]. By helping to quickly and accurately identify abnormal behavior, these systems offer strong tools. They can be used in areas like surveillance, security, healthcare, and more. This effectively addresses potential threats. By automating the identification process, these systems lessen the workload on human operators. They

also improve the speed and accuracy of surveillance systems. This helps with better monitoring and management of abnormal behavior. The use of this technology has great potential. It can improve public safety and system efficiency in many sectors[2].

The rise of deep learning technology has greatly expanded research opportunities. Deep learning methods can automatically find and understand high-level features in complex data. This ability helps in detecting unusual behavior. OpenPose[4] is a technology that focuses on human pose estimation. It provides detailed information about human movement by detecting many key points. OpenPose is very good at monitoring changes in posture. It is especially useful for finding abnormal behaviors like falls. This is because it can capture small movements in posture. However, OpenPose is quite complex. It requires a lot of hardware resources and computing power. It may not work well in difficult situations, such as when something blocks the view. In contrast, LSTM (Long Short-Term Memory) networks[5] are a type of recurrent neural network. They are designed for working with sequence data. These networks have been widely used to model how abnormal behavior changes over time. By using their long-term memory units, LSTMs can keep important long-term information. They also perform well in capturing complex patterns in time-series data.

However, LSTMs can face challenges. These challenges include gradient vanishing or explosion. This often happens when they work with long sequences. As a result, their performance may not be very good in situations where abnormal behavior changes quickly [6]. On the other hand, the YOLO (You Only Look Once) algorithm provides efficient object detection[7]. It works by dividing the image into grids. Then, it predicts targets at the same time. This allows for real-time processing and a global view of the image. YOLO is strong in its speed and adaptability. This enables it to perform very well in real-time surveillance applications. However, it can face challenges. This happens when it has lower localization accuracy. This issue often occurs with small or closely packed targets. The YOLO algorithm was chosen for the goals and requirements of this research. Its ability to work in real time and its efficiency match the need for quick monitoring of abnormal behavior. Furthermore, its global perception feature helps it adapt to different situations and complex environments. Finally, its simple network structure helps reduce the cost and time needed for system development. After thinking carefully about these factors, we chose to use the YOLO algorithm as the main framework for detecting abnormal behavior in this study. Our proposed model, HGO-YOLO, is based on YOLOv8. It aims to improve the performance and accuracy of detecting abnormal behavior.

This paper shows the main contributions. These contributions are as follows:

- 1) The HGNetv2 architecture is utilized for hierarchical feature extraction within the backbone network, with the goal of enhancing its capability to process complex image data. This architecture incorporates multiple convolutional layers with diverse filter sizes, allowing the network to capture a broad spectrum of features and thus improving its overall performance.
- 2) Replacing Conv convolution with GhostConv not only effectively reduces the number of computations and parameters but also excels in efficiently extracting feature information.
- 3) Design an OptiConvDetect detection head that not only leverages the superior performance of decoupled heads but also reduces model parameters and computational costs, making the model more lightweight and efficient.

The paper is structured as follows: Section 2 introduces related work, with a particular focus on state-of-the-art methods in recognizing human abnormal behavior. Section 3 provides a detailed description of our proposed HGO-YOLO. Section 4 validates the model's effectiveness through experiments. Finally, Section 5 presents the conclusion.

2. Related Work

To address the challenges of multiscale targets and complex image backgrounds, researchers have proposed various improved algorithms[8]. To address the issue of multi-scale object detection, some researchers have focused on reconstructing the feature pyramid structure. For instance, Liu et al. [9] developed the PDT-YOLO algorithm based on YOLOv7-tiny. They integrated the PANet structure into the head component, incorporating bottom-up augmentation routing and adaptive feature pooling operations. This method allows interaction and fusion between features at different levels. It improves detection accuracy for objects of different sizes. In addition, in the study[10], QAFPN was suggested to fully combine feature information from four layers of different sizes. This stops information from being lost or becoming less useful. It also reduces the difference between layers that are not next to each other. As a result, the model becomes better at detecting objects of various sizes. These studies improve detection accuracy through cross-level feature fusion and adaptive feature pooling. They also make the feature maps more expressive and help the model detect objects more efficiently. However, these improvements come with some downsides. The model becomes more complex, which leads to higher computational costs during training and inference.

To meet the needs for real-time performance, researchers often use lightweight backbone networks. Cui et al.[11] combined MobileNet with the YOLOv4 framework. This created a lightweight backbone for feature extraction. They designed multi-scale feature fusion modules. These modules add more feature information. As a result, they created a lightweight object recognition model. This model supports fast and accurate detection of targets in different situations. In a similar way, [12] introduced LFF-YOLO. It is based on YOLOv3 and uses ShuffleNetv2 as the backbone. This approach achieved big reductions in parameters and inference speed. However, these

lightweight networks have a limited number of layers and parameters. This can limit their ability to capture complex features and details. As a result, it may lead to not representing intricate patterns well enough.

Additionally, some researchers use lightweight convolutions. This helps to decrease the number of parameters. Qin et al. [13] added depth-separable convolution to YOLOv3. This change significantly reduces the number of parameters and the amount of computation. Importantly, it does this without losing accuracy. This allows the effective use of deeper and wider neural networks. Similarly, [14] introduced the DualConv lightweight deep neural network, which cut the parameters of MobileNetV2 by 54%. Zhao et al.[15] used ShuffleNetv2 as the backbone for extracting features from pomegranates. They utilized group convolution to reduce computational load and increased channel interaction through random channel ordering. These lightweight techniques lower computation and parameter counts, enhancing processing speed and efficiency, but they may also decrease accuracy and limit feature extraction capabilities.

3. Methods

3.1 YOLOv8 Algorithm

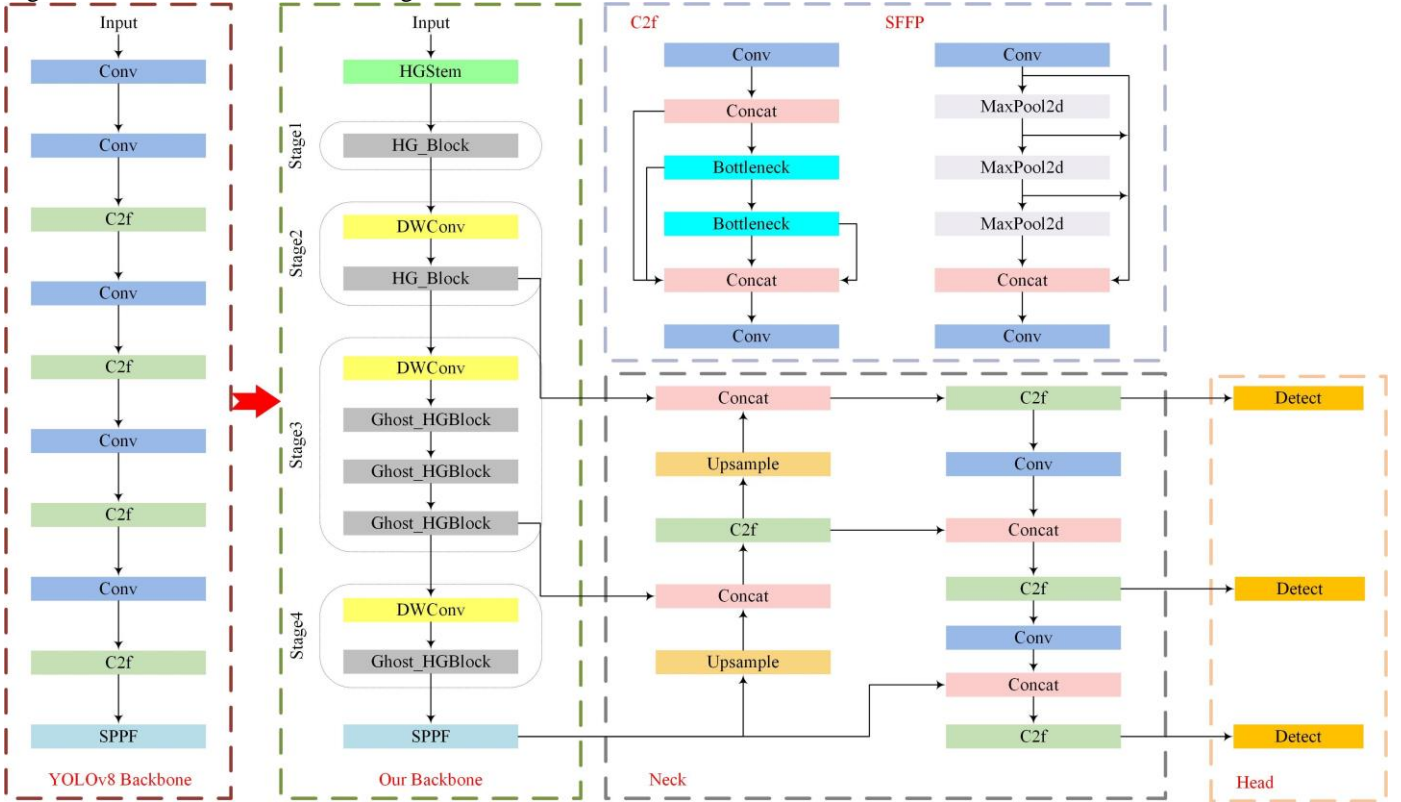
The YOLO series algorithms exhibit a high degree of similarity. The YOLOv8 model used in this study is primarily composed of three components: the backbone, neck, and head, as shown in Fig 1.

The backbone network is tasked with extracting feature information from the input image. YOLOv8 adopts the C2f(Cross Stage Partial Network Bottleneck with 2 Convolution) structure to enhance feature extraction efficiency and facilitate richer gradient flow information, thereby improving the understanding of image content while maintaining a lightweight design. Additionally, the SPP (Spatial Pyramid Pooling) mechanism is enhanced to SPPF through serial and parallel modifications. YOLOv8's neck network adopts a similar architecture to FPN (Feature Pyramid Network) used in PANet, effectively integrating features of different scales, particularly excelling in multi-scale object detection tasks. The YOLOv8 head network is responsible for detecting targets and providing the coordinates and categories of the detection box. To achieve this, it employs the Decoupled-Head structure, which separates the regression and prediction branches. Additionally, it integrates the integral form representation from the Distribution Focal Loss strategy to manage the regression branch. This strategic approach enhances target detection performance by transforming coordinate predictions from a deterministic single value to a distribution.

3.2 HGO-YOLO

To enhance accuracy and facilitate rapid recognition of abnormal behaviors, we introduce the HGO-YOLO method, whose architecture is depicted in Fig 1. The backbone structure consists of HGStem, HG_Block, DWConv, Ghost_HGBlock, and SPPF modules. Regarding the head network, we propose a novel detection head named OptiConvDetect, which reduces model parameters and computational costs by employing parameter sharing and PConv convolution layers. HGO-YOLO uses the MPDIoU loss function, enhancing its performance.

Fig 1: HGO-YOLO Architecture Diagram.



3.2.1 HGNetv2

The HGNetv2 network captures multi-level information in graph structures by extracting features and aggregating information at different scales. It utilizes graph convolution operations to aggregate relationships between nodes, adaptively adjusts information aggregation strategies, and enhances feature representation capability and model robustness. The structure diagram of HGNetv2 is shown in Fig 1.

As shown in Figure 1, the structure of HGNetv2 is composed of multiple HGBlock. The specific structure of the HGBlock module is illustrated in Fig 2. The HGBlock module enhances feature representation capabilities through multiple layers of convolution, feature concatenation, channel compression and expansion, and residual connections, with the ability to handle multi-scale features. The module starts with an input feature map X of dimensions $c \times h \times w$. By stacking $Layer_num$ convolutional blocks, each consisting of a convolutional layer, batch normalization (BN), and an activation function (ReLU), the module captures features at different scales due to varying receptive fields of these convolutional blocks. The outputs of these convolutional blocks are denoted as $Y_0 \sim Y_{Layer_num-1}$.

After passing through all convolutional layers, the module concatenates the output feature maps along the channel dimension to preserve multi-scale feature information, as described by the following formula:

$$Z = Concat(Y_0, Y_1, \dots, Y_{Layer_num-1}) \quad (1)$$

The concatenated feature map has dimensions $(Layer_num \times c_{mid}) \times h' \times w'$, where c_i is the number of output

channels of each convolutional block, and h' and w' are the height and width after the convolution operations. This concatenated feature map is then passed through a convolutional layer to compress the number of channels to $out_channels/2$. This step reduces computational complexity and enhances feature compactness, resulting in the feature map Z' . This step reduces computational complexity and enhances feature compactness, resulting in the feature map Z'' . This adjustment in the number of channels facilitates feature fusion and channel adaptation. By using a shortcut connection, the aggregated output is combined with the original input X , ensuring the retention of original information within the network to mitigate information loss. Finally, the entire module undergoes batch normalization and activation to further improve training stability and model generalization.

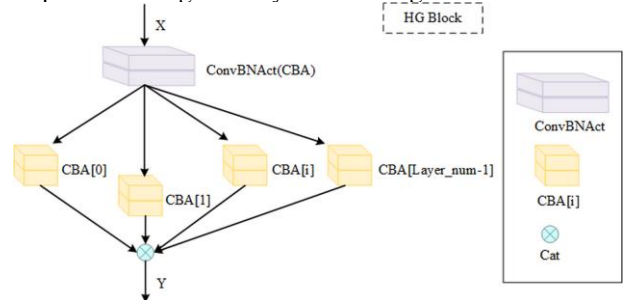


Fig 2: HGBlock module structure diagram.

3.2.2 Ghost_HGBlock

To reduce the model's size and computational load while maintaining performance, I prioritized lightweight solutions. Han et al.[16] extensively explored the information within feature maps and introduced a more lightweight Ghost convolution (GhostConv) module by fully leveraging

feature map redundancy. The main difference between traditional convolution (Conv) and GhostConv lies in the number of parameters and computational efficiency, as depicted in Fig 3, providing a clear illustration of their operations. Traditional convolution, as shown in Fig 3(a), takes an input feature map $X \in R^{c \times h \times w}$ where c represents the number of input channels, and h and w are the input height and width, respectively. The convolution operation is mathematically described by Eq(2), yielding an output n -dimensional feature map $Y \in R^{h' \times w' \times n}$. Here, the convolution kernel $f \in R^{c \times k \times k \times n}$ (with k as the size of the convolution kernel), and b signifies the bias term. Therefore, the computational cost of this layer is denoted by $FLOP_{S1}$ as shown in Eq (3). In traditional convolution, each input channel has corresponding convolutional kernel weights and biases, and typically, n and c are large, resulting in a relatively large number of parameters and computational load.

$$Y = X * f + b \quad (2)$$

$$FLOP_{S1} = n \times h' \times w' \times c \times k \times k \quad (3)$$

The operation flow of the Ghost module consists of three steps: Firstly, The input image is convolved once by halving the number of channels and using Conv with a convolution kernel size of 1×1 , integrating features to generate a condensed feature map of the input feature layer. Secondly, a 3×3 convolution kernel is applied to the condensed feature map obtained from the previous step. This step is aimed at performing a cost-effective operation, resulting in a redundant feature map known as cheap operations. Finally, the condensed feature map and the redundant feature map generated in the first two steps are concatenated together. This concatenation process produces the final output feature map. For a visual representation of this structure, please refer to Fig 3(b).

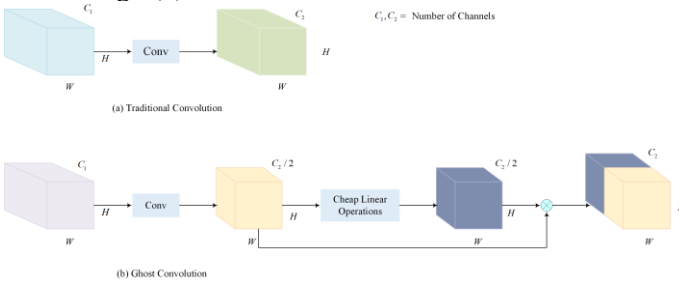


Fig 3: Ghost convolution vs. standard convolution.

The Ghost module operates by taking an input feature map $X_1 \in R^{c \times h \times w}$ and producing an output feature map $Y_1 \in R^{h' \times w' \times m}$ using a convolution kernel $f_1 \in R^{c \times k \times k \times m}$ (where $m < n$). For simplicity, the bias term b is omitted. The output Y_1 then undergoes $s-1$ group convolution operations with a kernel size of $d \times d$, which is customizable. This results in $s-1$ feature maps of size $m \times h' \times w'$. Finally, these feature maps are added to Y_1 to obtain a feature map of size $n \times h' \times w'$. The computational

cost of the Ghost module, denoted as $FLOP_{S2}$, can be calculated using Eq (4).

$$FLOP_{S2} = \frac{n}{s} \times h' \times w' \times c \times k \times k + (s-1) \times h' \times w' \times \frac{n}{s} \times d \times d \quad (4)$$

The ratio of computational cost between the two approaches can be expressed using Eq (5).

$$\frac{FLOP_{S1}}{FLOP_{S2}} = \frac{c \times k \times k}{\frac{1}{s} \times c \times k \times k + \frac{(s-1)}{s} \times d \times d} \approx \frac{s \times c}{s + c - 1} = \frac{s}{1 + \frac{s-1}{c}} \approx s \quad (5)$$

It can be observed that the computational cost of GhostConv is reduced to $1/s$ of the original cost when compared to traditional convolution.

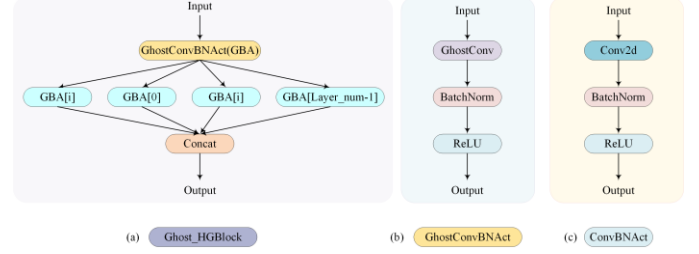


Fig 4: (a) The internal structure of the Ghost_HGBlock module. (b) Ghost Convolution with Batch Normalization and Activation (orange in Ghost_HGBlock). (c) Convolution with Batch Normalization and Activation.

Replacing ConvBNAct with GhostConvBNAct significantly enhances network performance. GhostConvBNAct boosts the ability to capture multi-scale features by generating both main features and pseudo-features, while simultaneously reducing computation and parameter count. This makes the network more efficient in handling large-scale data. Additionally, this structure improves feature expression capabilities and accuracy, making it well-suited for resource-constrained environments, such as mobile devices or embedded systems.

3.2.3 OptiConvDetect

To improve the accuracy of predicting object classes and locations, YOLOv8 employs a decoupled detection head module that separates the classification and regression branches, as shown in Fig 5. This module divides the object detection task into two main branches: one for object classification and the other for location regression. During detection, spatial feature extraction starts with two convolutional layers, followed by processing the output channels with final convolutional layers to generate prediction information. Assuming the input feature map is X , after processing through two convolutional layers, the resulting feature map is X' , which is then processed through regression branch R and classification branch C to produce the final predictions:

$$R(X') = Conv_{reg}(X') \quad (6)$$

$$C(X') = Conv_{cls}(X') \quad (7)$$

However, integrating three detection heads leads to a total of 12 3×3 convolutional layers and 6 1×1 convolutional layers, significantly increasing the model parameters, making the detection head account for 41.4% of YOLOv8's GFLOPs.

To address this challenge, we propose an optimized model structure by introducing parameter sharing in the detection

head, called OptiConvDetect. Our strategy avoids separating detection by introducing a single PConv convolutional layer P , and then adding a convolutional layer $Conv_{opt}$ for the output channels[19]. This optimization allows for parameter sharing, achieving:

$$P(X) = PConv(X) \quad (8)$$

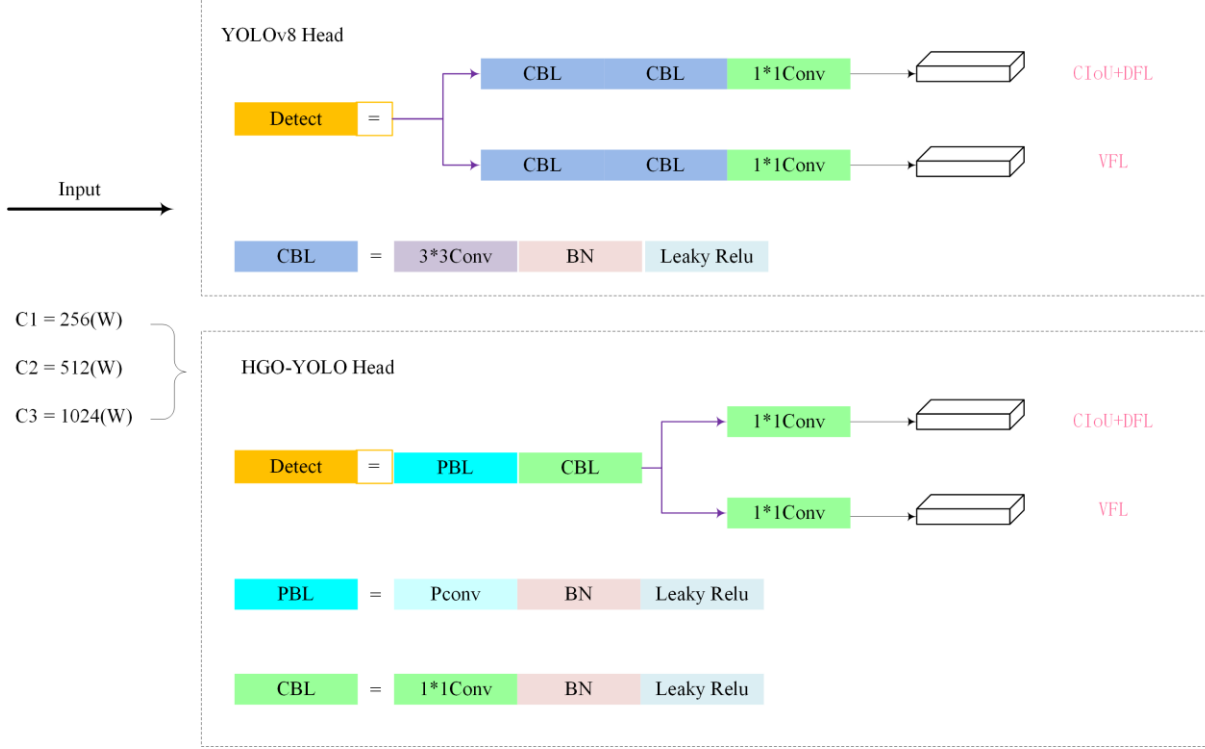


Fig 5: YOLOv8 Head vs. HGO-YOLO Head.

In Fig 5, we introduce an improved convolutional layer design in the detection head module to reduce model complexity by sharing convolutional layer parameters. The feature extraction module consists of PConv and 1x1 convolutional layers, which are reused across different detection heads to achieve parameter sharing. These feature extraction modules can be reused on different input feature maps, further facilitating parameter sharing. For regression prediction, assuming the feature map X is processed through shared PConv and 1x1 convolutional layers to obtain X'' , the regression prediction \hat{B} is generated as follows:

$$\hat{B} = DFL(Conv_{reg}(X'')) \quad (10)$$

Similarly, for classification prediction, the classification prediction \hat{C} is obtained:

$$\hat{C} = Conv_{cls}(X'') \quad (11)$$

During forward propagation, parameter sharing for feature extraction and prediction generation is reused across each detection head. Additionally, the model dynamically computes and updates anchors A and strides S based on the input shape, allowing the model to share and adjust parameters under different input conditions, thereby enhancing model flexibility and efficiency:

$$Conv_{opt}(P(X)) = Conv(P(X)) \quad (9)$$

This optimization aims to streamline the model structure while maintaining prediction accuracy, ultimately improving efficiency and reducing computational complexity.

$$A, S = DynamicAnchorStride(X, shape) \quad (12)$$

This design allows the model to automatically adjust parameters while handling different input sizes, maintaining efficient computation and accurate predictions.

4. Experimental Analysis and Visualization

4.1 Dataset Description

This study uses a dataset that is composed of six publicly available datasets, cited as follows:

1. Fall Dataset: This includes the UR Fall Detection Dataset, the Fall Detection Dataset, the Multiple Cameras Fall Dataset, and segments of the COCO Dataset.
2. Fight Dataset: This comprises the Surveillance Camera Fight Dataset, A Dataset for Automatic Violence Detection in Videos, and the Real Life Violence Situations Dataset.
3. Smoking Dataset: This dataset comprises 2912 images sourced from real-life scenarios via the Internet.

For video streams obtained from public datasets, we initially conducted frame-by-frame processing to convert the video data into images. Due to the potential generation of numerous highly similar photos during this process, we implemented dataset filtering to reduce redundant data. This resulted in a total of 3224 images in the battle dataset and 4065 images in the fall dataset. During the annotation process of these 10,201 images, we established detailed annotation standards and categorized the images into four classes: fall, fight, smoke, and person.

Subsequently, the labeled dataset was divided into train, validation, and test sets in a ratio of 8:1:1 to assess the effectiveness of the HGO-YOLO algorithm.

4.2 Experimental Setup

To comprehensively evaluate the performance of the HGO-YOLO algorithm, we implemented several algorithms, including basic versions of YOLO (v5, v6, v7, v8, v9, v10, v11), and RT-DTETR, all developed in PyTorch. We conducted a comparative analysis of their performance against the improved YOLOv8n. The experimental setup utilized an Intel(R) Xeon(R) Silver 4310 CPU @ 2.10GHz, NVIDIA A100 80GB PCIe GPU, and Ubuntu 20.04.2 operating system. During the network model training phase, we configured the number of training iterations to 200 and the batch size to 32. To ensure consistency in the evaluation framework, we adopted the models and extended hyperparameters defined in the original repository. This approach was chosen to prevent any confusion. Such confusion could come from using different hyperparameter settings. By doing this, it ensures that the experiments can be compared easily. It makes the results more trustworthy.

4.2 Evaluation Indicators

To fairly evaluate how well the HGO-YOLO model works, this study uses common measures. These are mAP, FPS, and GFLOPs. Mean Average Precision (mAP) is an important measure. It helps to check how well object detection models work, especially with many classes. It gives a full evaluation of how well the model can find objects in different classes. It does this by calculating the Average Precision (AP) for each class. The calculation formula is given in (13). AP comes from the precision-recall curve (PR curve) that the model creates. This curve shows the balance between precision (the ratio of true positive results to all positive results) and recall (the ratio of true positive results to all actual positive cases). The confidence threshold of the model changes as this balance is shown. The formula for AP is below:

$$Precision = \frac{TP}{TP + FP} \quad (12)$$

$$Recall = \frac{TP}{TP + FN} \quad (13)$$

$$AP = \sum_n (R_n - R_{n-1}) P_n \quad (14)$$

TP stands for True Positives. It is the number of cases that the model correctly classified as positive. FP stands for False Positives. It is the number of cases where the model incorrectly said something was positive, but it was actually negative. FN (False Negatives) represents the number of instances incorrectly classified as negative by the model when they are positive.

GFLOPs represent the computational load during the inference phase. Lower GFLOPs indicate faster inference and reduced computational requirements, making the model more efficient, especially in scenarios where real-time recognition or processing is necessary.

4.3 Ablation Study

To comprehensively evaluate the impact and contributions of various module improvements in the HGO-YOLO model, we conducted ablation experiments. Using the same dataset and training parameters, we analyzed the effects of these

improvements on the detection results. The specific details are presented in Table 1. The baseline model (b) achieved a performance of 33 FPS and mAP@0.5 of 84.4, with mAP@0.5 values of 83.8, 92.4, 75.0, and 86.5 for the categories of fall, fight, smoke, and person, respectively.

In Table 1 we compared five different configurations of the model:

- H-YOLO: With the introduction of HGNetv2, the FPS significantly increased to 54, and the overall mAP@0.5 improved to 85.9. Notably, the detection performance for the fight and person categories showed significant improvement, indicating that HGNetv2 contributes substantially to enhancing both the speed and accuracy of the model.
- HG-YOLO: When the standard convolution in the HGNetv2 backbone was replaced with GhostConv, although the FPS slightly decreased to 52, the mAP@0.5 increased to 87.1. This was particularly evident in the improved detection accuracy for the fall, fight, and person categories, demonstrating that the GhostConv module effectively enhances the computational efficiency and detection accuracy of the model.
- O-YOLO: With the introduction of the OptiConvDetect detection head alone, the FPS was 51, and the mAP@0.5 was 86.2. There was a noticeable improvement in the mAP@0.5 for the fight and person categories, indicating that the OptiConvDetect detection head significantly contributes to improving detection accuracy.
- HO-YOLO: The system uses HGNetv2 and the OptiConvDetect detection head. The FPS reached 52, and the mAP@0.5 was 86.0. This setup did very well in many categories. It performed especially well in the person category. This shows that the two improvements work well together to balance speed and accuracy.
- HGO-YOLO: The model includes HGNetv2, the GhostConv module, and the OptiConvDetect detection head. It reached the best performance with an FPS of 56. The mAP@0.5 was 87.4. The mAP@0.5 values for the fall, fight, smoke, and person categories were 85.1, 93.1, 75.4, and 96, respectively, demonstrating the significant contributions of each module to the overall performance and detection accuracy of the model. This indicates that the introduction and optimization of each module play a crucial role in enhancing the detection performance and efficiency of the HGO-YOLO model.

4.4 Analysis of Experimental Results at Different Scales

The experimental results are summarized as follows: Table 2 presents the outstanding detection mAP results achieved by the HGO-YOLO model throughout the experiment. The results indicate that the model's performance improvement is closely tied to its scale. Smaller models exhibit more substantial improvements in parameter size. When measured by mAP@0.5, YOLOv8n and YOLOv8s increased by 3 percentage points and 3.7 percentage points, respectively. When measured by mAP@0.95, YOLOv8n increased by 2.9 percentage points. It is noteworthy that although the parameters of the HGO-YOLOs model are three times that of HGO-YOLOn, the performance of HGO-YOLOn is comparable to that of HGO-YOLOs. A similar improvement trend was also observed in YOLOv8x, a

Table 1: Ablation study results, the baseline YOLOv8n model.

	Models			FPS	mAP@0.5					size	
	H	G	O		ALL	fall	fight	smoke	person	GFLOPs	#Param.
b				33	84.4	83.8	92.4	75.0	86.5	8.9	6.2MB
1	✓			54	85.9	82.7	93.7	73.5	93.5	6.9	4.9MB
2	✓	✓		52	87.1	83.9	94.7	74.8	95.1	6.8	4.8MB
3			✓	51	86.2	83.7	93.2	73.3	94.5	5.5	5.1MB
4	✓		✓	52	86.0	83.2	93.3	73.3	94.2	4.3	3.8MB
5	✓	✓	✓	56	87.4	85.1	93.1	75.4	96	4.3	4.6MB

Table 2: Comparing experimental results of different scales with YOLOv8 detection baseline.

Model	#Param.	GFLOPs	FPS	Detection				Accuracy			
				Precision	Recall	mAP@0.5	mAP@0.95	fall	fight	smoke	person
YOLOv8n	6.2MB	8.9	33	84	79.1	84.4	57.5	83.8	92.4	76	85.5
HGO-YOLOn	4.6MB	4.3	56	87.1	81.1	87.4	60.4	85.1	93.1	75.4	96
improvement	1.6	4.6	23	3.1	2	3	2.9	1.3	0.7	-0.6	10.5
YOLOv8s	22.5MB	28.4	13	85	80.1	84	58.5	82.7	93.3	77.5	82.4
HGO-YOLOs	13.9	16	15	86.6	82.3	87.7	61.2	84.5	94.8	77	94.4
improvement	8.6	12.4	2	1.6	2.2	3.7	2.7	1.8	1.5	-0.5	12
YOLOv8m	52MB	78.7	6	86.7	80.5	86.2	60.2	85.3	93.1	80.8	85.5
HGO-YOLOm	30.5MB	43.3	7	89	82.8	88.6	62.6	86.6	95	78.8	94.1
improvement	21.5	35.4	1	2.3	2.3	2.4	2.4	1.3	1.9	-2	8.6
YOLOv8l	87.6MB	164.8	3	86.6	79.8	86.9	60.4	85.2	95.1	81.2	85.9
HGO-YOLOl	49.5MB	86.5	5	88.7	83.7	89	63.4	88	95.2	80	92.9
improvement	38.1	78.3	2	2.1	3.9	2.1	3	2.8	0.1	-1.2	7
YOLOv8x	136.7MB	257.4	2	84.3	81.8	86.5	60.9	85.3	94.5	81.5	84.9
HGO-YOLOx	77MB	136.5	3	89.4	83.8	89.4	62.9	87.5	95.4	80.3	94.3
improvement	59.7	120.9	1	5.1	2	2.9	2	2.2	0.9	-1.2	9.4

Fig 6: Compared with the baseline detection performance of HGO-YOLO.

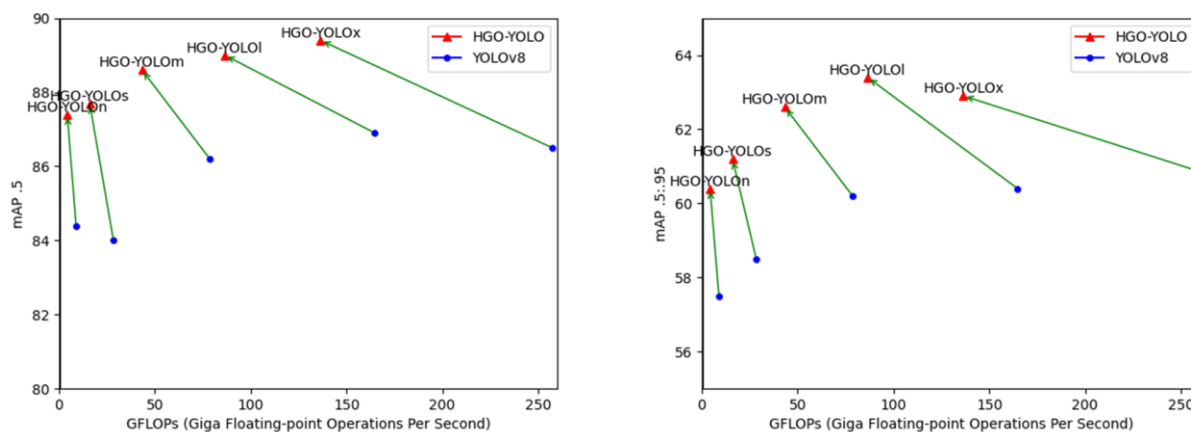


Table 3: Comparison of the Improvement Effect of the Lightweight Detector Head at Different Positions.

OptiConvDetect	GFLOPs	Accuracy				
		fall	fight	smoke	person	ALL
Conv-Conv	4.3	83.8	93.5	73.9	94.1	86.3
Conv-PConv	4.2	85.7	94.5	73.1	94.2	86.9
PConv-Conv	4.3	85.1	93.1	75.4	96	87.4
PConv-PConv	4.1	86.2	93.3	73.0	94.4	86.7

Table 4: Comparison with other methods, the maximum values are highlighted in bold.

Model	#Param.	FPS	Accuracy				
			fall	fight	smoke	person	ALL
RT-DETR	40.5M	8	78.2	88.9	74.7	82.9	81.2
YOLOv5n	5.3M	32	83.1	91.9	76.8	86.5	84.6
YOLOv6n	8.7M	36	84.3	92.1	73.4	86.8	84.1
YOLOv7-tiny	12.3M	27	82.8	90.3	74.5	85.2	83.2
YOLOv8n	6.3M	33	83.8	92.4	76.0	85.5	84.4
YOLOv9t	6.1M	10	84.5	92.5	76.9	87.3	85.1
YOLOv10n	5.8M	41	84.0	92.0	72.3	91.9	85.0
YOLOv11n	5.3M	16	84.6	91.5	77.2	86.7	85.0
HGO-YOLO	4.6M	56	85.1	93.1	75.4	96.0	87.4

model with 136.7 million parameters. Table 2 clearly illustrates the increase in model complexity, as measured by the number of parameters, floating-point operations, and frames per second (FPS). Thanks to the ingenuity of the HGO-YOLO model, significant improvements have been achieved across the three standards of the model at different scales. Even for the larger YOLOv8l model, its performance improvement reached 89% mAP@0.5, showcasing the effectiveness of the HGO-YOLO approach. To enhance the presentation of our research findings, we conducted a thorough analysis of the performance improvements achieved by each model. We aim to vividly illustrate the performance differences between models of different scales operating under identical conditions by visualizing the performance curves, as shown in Fig 6.

4.5 Analysis of PConv and Conv Substitution Positions

Table 3 compares the performance of four different replacement positions on the OptiConvDetect detector head. The results indicate that the PConv-Conv model achieved the highest overall accuracy at 87.4%, albeit with a relatively high computational cost. It notably performed well in detecting smoke anomalies with an accuracy of 75.4%. On the other hand, the Conv-PConv model, positioned differently, had slightly lower computational complexity and showed an advantage in the fall category. However, it experienced a 2.3% decrease in accuracy for the smoke category, resulting in a 0.5% drop in overall accuracy. The experiments conducted reveal that beginning with a conventional convolutional layer can result in the loss of intricate information during the feature extraction process. Transitioning to PConv can sometimes result in convolutional layers failing to recover or emphasize essential details from the original input, reducing accuracy in detecting small smoke targets. In the PConv-PConv experiment, while the "fall" category showed the best performance, the "smoke" category had the lowest accuracy. This is likely due to the exclusive use of PConv, which may limit the diversity of features and richness of information, preventing the model from fully capturing the data's complexity.

Although PConv excels in handling occlusions and extracting features from specific regions, relying on it alone can reduce the model's flexibility and adaptability across different tasks. On the other hand, the Conv-Conv model yielded the lowest overall accuracy, showing no clear advantage in any anomaly behavior. This is likely due to traditional convolutional layers treating all input features equally, without focusing on more critical parts of the input.

For tasks requiring high accuracy with manageable computational demands, the PConv-Conv model stands out as an optimal choice. It combines partial convolution (PConv) for initial feature extraction with traditional convolution (Conv) to refine and process features. PConv is effective in managing incomplete data or attention mechanisms, while the subsequent Conv layer enhances feature representation for better target detection. This hybrid approach improves the model's ability to detect and localize targets in complex scenes while maintaining computational efficiency.

4.6 Comparison with Other Methods

To comprehensively evaluate the performance of HGO-YOLO, we conducted a series of experiments on the dataset and detailed the detection results in Table 4. The experimental results show that HGO-YOLO achieves a mAP of 87.4 while maintaining an excellent 56 FPS, leading in both metrics. Additionally, compared to RT-DETR[18], HGO-YOLO shows significant improvements in mAP and detection speed, with a 6.2 mAP increase and 7x FPS improvement. Compared to YOLOv5n, YOLOv6n, YOLOv7-tiny, and YOLOv8n, our model achieves higher mAP scores of 2.8, 3.3, 4.2, and 3, respectively. In terms of detection speed, HGO-YOLO's 56 FPS is the highest. It is noteworthy that our model performs most accurately in detecting anomaly behaviors such as fall and fight. Overall, HGO-YOLO effectively detects anomaly behaviors while maintaining a relatively fast detection speed.

4.7 Experiments with Different Loss Functions

The paper investigates various types of IoU[19] loss functions and conducts experiments to determine which one can achieve optimal performance. Several loss functions were evaluated,

including DIoU loss[20], CIoU loss[21], MPDIoU loss[22], and Inner-CIoU loss[23]. Table 5 presents the comparison results. Our model achieved the highest mAP of 87.4% when utilizing MPDIoU as the loss function for HGO-YOLO. MPDIoU was determined to be more suitable for our model compared to the other mentioned loss functions[24].

Table 5: Comparison of Various Losses

Loss	DIoU	MPDIoU	CIoU	Inner-CIoU
mAP	86.9	87.4	87.1	86.4

4.8 Test

To evaluate the real-time detection capabilities of the improved models on different devices, we deployed YOLOv8 and HGO-YOLO on both Raspberry Pi and NVIDIA and conducted tests. The results are shown in the table below:

Table 6: Real-Time Detection Performance of YOLOv8 and HGO-YOLO on Different Devices

Device	Model	FPS
Raspberrry Pi4	YOLOv8	0.638
	HGO-YOLO	0.833
NVIDIA Jetson Orin Nano	YOLOv8	13.33
	HGO-YOLO	33.33

From the table, it is evident that HGO-YOLO outperformed YOLOv8 on both devices, particularly on NVIDIA, where it achieved a frame rate of 33.33FPS, demonstrating significant real-time detection capability.

4.9 Visualization

To compare the performance of the HGO-YOLO model with the baseline model on the anomaly detection dataset, we conducted a series of visualizations. Fig 7 presents the prediction results of the YOLOv8n and HGO-YOLO models for the fall category using identical validation input. It is evident that HGO-YOLO exhibits higher confidence in accurately detecting complex poses, even in challenging conditions such as dark lighting and severe occlusions, when compared to YOLOv8n. These findings highlight HGO-YOLO's capability to provide more reliable performance for real-time detection systems.



Fig 7: A comparison of detection performance for the fall category between YOLOv8n and HGO-YOLO.

The detection performance of the HGO-YOLO algorithm for the fight category is illustrated in Fig 8. In indoor scenes with dim lighting and confined spaces (a) and (b), YOLOv8n's detection results exhibit low confidence and missed detections. The improved algorithm not only enhances detection

confidence but also swiftly and accurately identifies complex human movements. In scene (c) depicting a crowded fight scenario, swift and accurate detection of fighting behavior is crucial. HGO-YOLO achieves higher confidence levels compared to YOLOv8n, while YOLOv8n may produce false positive detections.



Fig 8: A comparison of the detection performance for the fight category between YOLOv8n and HGO-YOLO.

Fig 9 illustrates a comparison of smoke category detection results between YOLOv8n and HGO-YOLO. YOLOv8n exhibits false positives when detecting small targets, whereas HGO-YOLO performs exceptionally well. In image (c), captured at night, low illumination presents a challenge to the detectors. The comparison highlights that HGO-YOLO surpasses YOLOv8n in terms of detection confidence, with no false positives. The HGO-YOLO algorithm effectively enhances YOLOv8n's detection of small targets, improves resistance to background noise, and reduces both false alarm and miss rates.



Fig 9: Smoke category detection performance comparison between YOLOv8n and HGO-YOLO.

5. Conclusion

This study focuses on the application performance of the improved HGO-YOLO model in real-time detection. We conducted systematic performance testing by deploying HGO-YOLO on both Raspberry Pi and NVIDIA platforms. The results indicate that HGO-YOLO outperformed YOLOv8 on both devices, particularly on the NVIDIA platform, where it achieved significantly higher frame rates and lower latency, demonstrating its exceptional real-time detection capabilities. However, while HGO-YOLO performs well in various scenarios, it does have certain limitations. For instance, its accuracy may be compromised when detecting small smoking

targets. Additionally, its performance on resource-constrained devices may not be as optimal as on high-performance platforms. Therefore, future research should focus on further optimizing HGO-YOLO to enhance its stability and accuracy across different application scenarios, while also considering hardware resource constraints.

References

- [1] Luo, Z., Jia, S., Niu, H., Zhao, Y., Zeng, X., & Dong, G. (2024). Elderly Fall Detection Algorithm Based on Improved YOLOv5s. *Information Technology and Control*, 53(2), 601-618.
- [2] Rezaee, K., Rezakhani, S. M., Khosravi, M. R., & Moghimi, M. K. (2024). A survey on deep learning-based real-time crowd anomaly detection for secure distributed video surveillance. *Personal and Ubiquitous Computing*, 28(1), 135-151.
- [3] Shamim, R., Alfurhood, B. S., Agarwal, T., & Mallik, B. B. (2024). YOLOv8 for Anomaly Detection in Surveillance Videos: Advanced Techniques for Identifying and Mitigating Abnormal Events. *Mathematical Modeling for Computer Applications*, 317-349.
- [4] Cao, Z., Simon, T., Wei, S. E., & Sheikh, Y. (2017). Realtime multi-person 2d pose estimation using part affinity fields. In *Proceedings of the IEEE conference on computer vision and pattern recognition* (pp. 7291-7299).
- [5] Staudemeyer, R. C., & Morris, E. R. (2019). Understanding LSTM—a tutorial into long short-term memory recurrent neural networks. *arXiv preprint arXiv:1909.09586*.
- [6] Wu, J., Wang, J., Zhan, A., & Wu, C. (2021). Fall detection with cnn-casual lstm network. *Information*, 12(10), 403.
- [7] Redmon, J. (2016). You only look once: Unified, real-time object detection. In *Proceedings of the IEEE conference on computer vision and pattern recognition*.
- [8] Wang, Yaru, et al. "MCI-GLA Plug-in Suitable for YOLO Series Models for Transmission Line Insulator Defect Detection." *IEEE Transactions on Instrumentation and Measurement* (2024).
- [9] Liu, R., Huang, M., Wang, L., Bi, C., & Tao, Y. (2024). PDT-YOLO: A Roadside Object-Detection Algorithm for Multiscale and Occluded Targets. *Sensors*, 24(7), 2302.
- [10] Hu, W., Hu, Q., Pi, J., Huang, K., Li, W., & Wang, J. (2024, April). Dense Pedestrian Detection Algorithm Based on Multiscale Feature Fusion in YOLOv8. In *2024 5th International Conference on Computer Vision, Image and Deep Learning (CVIDL)* (pp. 1362-1366). IEEE.
- [11] Cui, J., Wang, D., Li, H., Zhang, W., Zhang, J., & Zhang, G. (2022, August). Lightweight of Intelligent Real-Time Detection Model Based on YOLO-v4. In *2022 2nd International Conference on Frontiers of Electronics, Information and Computation Technologies (ICFEICT)* (pp. 244-247). IEEE.
- [12] Qian, X., Wang, X., Yang, S., & Lei, J. (2022). LFF-YOLO: A YOLO algorithm with lightweight feature fusion network for multi-scale defect detection. *IEEE Access*, 10, 130339-130349.
- [13] Qin, Y. Y., Cao, J. T., & Ji, X. F. (2021). Fire detection method based on depthwise separable convolution and yolov3. *International Journal of Automation and Computing*, 18(2), 300-310.
- [14] Zhong, J., Chen, J., & Mian, A. (2022). DualConv: Dual convolutional kernels for lightweight deep neural networks. *IEEE Transactions on Neural Networks and Learning Systems*, 34(11), 9528-9535.
- [15] Zhao, J., Du, C., Li, Y., Mudhsh, M., Guo, D., Fan, Y., ... & Almodfer, R. (2024). YOLO-Granada: a lightweight attentioned Yolo for pomegranates fruit detection. *Scientific Reports*, 14(1), 16848.
- [16] Han, K., Wang, Y., Tian, Q., Guo, J., Xu, C., & Xu, C. (2020). Ghostnet: More features from cheap operations. In *Proceedings of the IEEE/CVF conference on computer vision and pattern recognition* (pp. 1580-1589).
- [17] Ma, X., Guo, F. M., Niu, W., Lin, X., Tang, J., Ma, K., ... & Wang, Y. (2020, April). Pconv: The missing but desirable sparsity in dnn weight pruning for real-time execution on mobile devices. In *Proceedings of the AAAI conference on artificial intelligence* (Vol. 34, No. 04, pp. 5117-5124).
- [18] Zhao, Y., Lv, W., Xu, S., Wei, J., Wang, G., Dang, Q., ... & Chen, J. (2024). Detsr beat yolos on real-time object detection. In *Proceedings of the IEEE/CVF Conference on Computer Vision and Pattern Recognition* (pp. 16965-16974).
- [19] Zhang, H., Wang, Y., Dayoub, F., & Sunderhauf, N. (2021). Varifocalnet: An iou-aware dense object detector. In *Proceedings of the IEEE/CVF conference on computer vision and pattern recognition* (pp. 8514-8523).
- [20] Zheng, Z., Wang, P., Liu, W., Li, J., Ye, R., & Ren, D. (2020, April). Distance-IoU loss: Faster and better learning for bounding box regression. In *Proceedings of the AAAI conference on artificial intelligence* (Vol. 34, No. 07, pp. 12993-13000).
- [21] Li, X., Wang, W., Wu, L., Chen, S., Hu, X., Li, J., ... & Yang, J. (2020). Generalized focal loss: Learning qualified and distributed bounding boxes for dense object detection. *Advances in Neural Information Processing Systems*, 33, 21002-21012.
- [22] Siliang, Ma, and Xu Yong. "Mpdious: a loss for efficient and accurate bounding box regression." *arXiv preprint arXiv:2307.07662* (2023).
- [23] Zhang, Hao, Cong Xu, and Shuaijie Zhang. "Inner-iou: more effective intersection over union loss with auxiliary bounding box." *arXiv preprint arXiv:2311.02877* (2023).
- [24] Zhao, C., Shu, X., Yan, X., Zuo, X., & Zhu, F. (2023). RDD-YOLO: A modified YOLO for detection of steel surface defects. *Measurement*, 214, 112776.